Transport in Porous Media (2026) 153:18
https://doi.org/10.1007/s11242-025-02267-0

Microstructure Simulation to Predict the Influence of Particle Properties on Permeability of Granular Porous Media

Paul Wendling[1,2] · Jennifer Sinclair Curtis[2] · Hermann Nirschl[1] · Marco Gleiss[1]

Received: 11 February 2025 / Accepted: 18 November 2025

Abstract
This work investigates the influence of particle shape and asperity height on the flow behavior of porous granular media using computational fluid dynamics (CFD). The developed framework includes the generation of random structured particle beds with LIGGGHTS using the Discrete Element Method (DEM) and the subsequent analysis of the pore space in terms of porosity and specific surface area. CFD is then applied to analyze the flow through the pore space at a Reynolds number of $Re = 1$. In the post-processing, the permeability of the granular porous media is derived and a significant influence of the particle shape and asperity height on the permeability and porosity can be seen. In the end, a comparative analysis of simulations results and analytical models based on Ergun and Carman-Kozeny is conducted. The study reveals that the Carman-Kozeny approach exhibits a remarkable capacity to replicate the influence of particle shape and surface asperity, while the Ergun approach demonstrates a more limited suitability.

Keywords Carman-Kozeny · Pore-scale simulation · Particle shape · Particle roughness

1 Introduction

The flow through granular porous media is of great importance for many industrial processes. The applications lay in the fields of cake filtration (Dong et al. 2009; Zhang et al. 2019), chemical catalysis (Bai et al. 2009; Li et al. 2021), nuclear fusion (Kumar et al. 2023) and battery technology (Marcato et al. 2022). Despite the relevance of these

✉ Marco Gleiss
marco.gleiss@kit.edu

Paul Wendling
paul.wendling@gmail.com

Jennifer Sinclair Curtis
jscurtis@ucdavis.edu

Hermann Nirschl
hermann.nirschl@kit.edu

[1] Institute of Mechanical Process Engineering and Mechanics, Karlsruhe Institute of Technology (KIT), 76131 Karlsruhe, Germany

[2] Department of Chemical Engineering, University of California, Davis, CA 94550, USA

Published online: 07 January 2026

processes, the design and analysis are still predominantly dependent on heuristics and experimentation (Mahdi et al. 2019). The commonly used empirical equations for the prediction of flow behavior in porous granular media contain significant uncertainties and can lead to considerable mistakes, if used in areas that are not directly proven by experiments (Rumpf et al. 1971).

The flow through granular porous media is highly dependent on the properties of the disperse phase (Steenweg et al. 2022). Until today, it is not possible to reliably derive porosity and permeability from the properties of particles because of the multiple influencing variables (Sorrentino 2007). Due to the limitations of the empirical equations, these parameters are still often determined in tedious laboratory experiments to design industrial applications. A more fundamental understanding is required regarding the effect of particle properties on the formation of granular porous media. The identification of the range of particle properties for which the commonly used empirical equations produce valid predictions would significantly aid process design. Pore-scale simulations are a valuable tool to investigate specific properties of particles, such as size distribution, shape and roughness. These simulations can then be compared with heuristic permeability predictions, which helps to assess the applicability of fundamental models (Marcato et al. 2022).

In recent years, the continuous increase in computational power and advances in numerical methods have significantly enhanced the use of particle and fluid simulations for analyzing complex flow behavior in granular porous media (Kumar et al. 2023). For example, the discrete element method (DEM) is used to randomly form a realistically packed bed of particles (Bai et al. 2009). Afterwards, the generated porous particle bed is processed in a CFD pre-processing tool to generate a computational grid to perform pore-scale simulations. The flow through granular porous media is then determined by the discrete solution of the Navier–Stokes equations. Many researchers have used this approach to study flow characteristics in packed beds. There have been studies on the pressure drop for monodisperse spherical and cylindrical particles (Bai et al. 2009), drag coefficients for polydisperse spherical particles (Rong et al. 2013), heat transfer in porous media (Kumar et al. 2023) and colloid transport within packed beds (Marcato et al. 2022). Numerous investigations focused on monodisperse spherical particles (Li et al. 2021; Schulz et al. 2019; Zhao et al. 2009). Initial studies have explored various particle shapes, including cylinders (Bai et al. 2009), ellipsoids (Rong et al. 2013), polydisperse particles (Marcato et al. 2022; Schulz et al. 2019) and bio-geochemically altered porous media (Hommel et al. 2018).

Other studies use Lattice Boltzmann simulations to examine the influence of particle size distribution and shape on porosity and tortuosity in randomly formed granular porous media (Kerimov et al. 2018; Xu et al. 2022). n both studies, particle shape is represented by spheroids, with particle-bed formation based on prolate or oblate grains. Their numerical analyses show that particle shape has a pronounced effect on permeability, while its influence on porosity remains minimal (Kerimov et al. 2018).

This study aims to investigate the effect of particle shape, specifically spheroids and surface roughness, defined by asperity height, on the porosity and permeability of granular porous media. The analysis is based on pore-scale simulations. To this end, we developed a simulation setup using the DEM software package LIGGGHTS for particle bed generation, enabling the simulation of various particle types. 2 distinct particle groups were selected for property analysis: elliptical particles to assess sphericity, and particles with surface asperities to investigate roughness. The generated particle beds serve as the foundation for pore-scale simulations using the finite volume method in the open-source CFD software OpenFOAM. Pressure loss, porosity, and bed permeability are then calculated and compared with analytical models, including Carman-Kozeny (Carman 1937) and Ergun (Ergun

et al. 1949). This makes it possible to assess the applicability of these models for non-spherical particles and particles with defined surface asperities.

2 Flow in Porous Media

Granular porous media is subject of relevance to a variety of engineering disciplines including oil and gas extraction (Li and Chen 2021), the drying of bulk materials (Qiu et al. 2015) and filtration (Anlauf et al. 2004). The fluid flow through porous systems is dependent on the existence of a driving force. This force may be caused by an applied pressure difference or by mass forces, such as gravity or centrifugal force (Sorrentino 2002). Depending on the flow pattern, a distinction is made between laminar and turbulent flow. The laminar flow in a porous system is governed by the Darcy equation:

$$\frac{\Delta p}{h_c} = \frac{\eta}{K} v_f \tag{1}$$

Here, Δp is the pressure loss of a particle bed, h_c is the bed height, η is the dynamic viscosity of the fluid, v_f is the superficial velocity and K is the permeability. Darcy's law can be derived from the Navier–Stokes equations by applying a volume-averaging procedure, as demonstrated by Whitaker (1986). The Darcy equation is valid for velocities that result in a Reynolds number below one (Nield et al. 2006).

The permeability represents a material parameter that characterizes the hydraulic resistance of a particle bed to fluid flow. It depends on five types of bed parameters for an incompressible, Newtonian flow: the average particle diameter x, particle distribution parameters q_i, particle shape coefficient ψ, bed porosity ε and the packing structure (Rumpf et al. 1971). The permeability is generally a tensor, but in the case of an isotropic granular porous media, it can be expressed as a scalar (Nield et al. 2006). The characterization of flow through granular porous media is predominantly supported by experimental evidence (Rumpf et al. 1971). The permeability is calculated with Darcy's law, as expressed in Eq. (1). This equation delineates the flow-pressure drop relationship through the particle bed (Sorrentino 2002). Nevertheless, it is challenging to evaluate the impact of individual particle characteristics through experimental observations. The primary reason for this is that when examining the influence of individual variables on a material parameter, such as porosity, all other influencing variables must be held constant. This is typically unfeasible during the experimental characterization of real porous systems due to the influence of individual bed parameters on one another.

There are many empirical equations that try to predict the permeability of granular porous media based on geometrical size parameters of the particle bed. The Carman-Kozeny model extends the Darcy equation and establishes a relationship between the geometric size of the pore system and permeability based on parallel channels and laminar flow. A considerable number of empirical (Sorrentino 2002) adhere to a similar fundamental structure:

$$K = \frac{x_{sv}^2}{C \cdot f(\varepsilon)} \tag{2}$$

Here, the permeability is related to a porosity function $f(\varepsilon)$, the Sauter diameter x_{sv}, and a constant C. A list of common permeability models can be found in Table 1.

Table 1 Porosity function $f(\varepsilon)$ and constant C of different permeability models [18]

Model	$f(\varepsilon)$	C
Carman-Kozeny	$\frac{(1-\varepsilon)^2}{\varepsilon^3}$	180
Rumpf-Gupte	$\varepsilon^{-5.5}$	5.6
Rumpf-Pahl	$\frac{1-\varepsilon}{\varepsilon^{4.55}}$	22.4
Richardson-Zaki	$\frac{1-\varepsilon}{\varepsilon^{4.65}}$	18

An important dimensionless quantity in fluid dynamics is the Reynolds number which allows to get information about the state of flow:

$$Re = \frac{\rho l_c v}{\eta} = \frac{\rho x_{sv} v_f}{\eta(1-\varepsilon)} \tag{3}$$

The Reynolds number is defined by the ratio of inertial and viscous forces and relates to the density of the fluid ρ, the dynamic viscosity η and a characteristic length l_c. For particle ensembles, the characteristic length is commonly represented by the Sauter diameter x_{sv}, which corresponds to the diameter of a sphere that shares the same surface-area-to-volume ratio as the particle size distribution (Rhodes 2008). A flow with a Reynolds number less than or equal to 1 corresponds to laminar flow through a granular porous media, while turbulent flow occurs at higher Reynolds numbers (Müller 2021).

The experimental investigation of Rumpf and Gupte (1971) focused on the uniform random packing of spherical particles, leading to a porosity function in the range of $0.3 \leq \varepsilon \leq 0.7$. In addition, the influence of geometric bed parameters on the permeability was investigated for $10^{-2} \leq Re \leq 10^2$. Table 1 shows a valid porosity function for $Re \leq 1$. Molerus et al. (1971) used the experimental data from Gupte and improved the prediction accuracy of the porosity function for lower porosities. Richardson and Zaki (1954) investigated the sedimentation of monodisperse particles and derived a porosity function whose exponent is based on a value of 4.65 for laminar flow.

For turbulent flows with higher Reynolds numbers, the influence of inertial resistance becomes more significant. It has been shown that across the entire velocity range, the pressure loss-velocity relationship for a porous bed can be expressed as the sum of frictional and inertial resistance components:

$$\frac{\Delta p}{h_c} = a_1 \eta v + b_1 \rho v^2 \tag{4}$$

Here, a_1 and b_1 are empirical parameters determined through experimental data and ρ is the density of the liquid. For predicting flow characteristics in granular porous media at higher Reynolds numbers, the Ergun equation serves as an effective model, incorporating both viscous and inertial contributions to the flow (Ergun et al. 1949):

$$\frac{\Delta p}{h_c} = 150 \frac{(1-\varepsilon)^2}{\varepsilon^3} \frac{\eta}{x_{sv}^2} v_f + 1.75 \frac{(1-\varepsilon)}{\varepsilon^3} \frac{\rho}{x_{sv}} v_f^2 \tag{5}$$

Here, the pressure loss exhibits an exponential relationship with flow velocity. In practice, the Ergun equation is applied across laminar, transient, and turbulent flow regimes.

3 Simulation Methodology

3.1 Generation of Porous Structures with DEM

The granular porous structures utilized for all simulations were generated using the open-source particle simulation software LIGGGHTS. The software is based on the numerical integration of Newton's equations of motion for particles that interact via short- or long-range forces with a variety of initial and/or boundary conditions (Lu et al. 2015). An important aspect of DEM is the contact modeling between particles. LIGGGHTS is founded on a soft-sphere model in which normal and tangential forces are integrated to predict particle–particle and particle–wall interactions. "In this study, we employ two distinct contact detection algorithms. For ellipsoids, the superquadratic library in LIGGGHTS enables efficient contact identification, following the approach of Podlozhnyuk et al. (2017). The contact detection relies on the concept of minimum bounding spheres, where the algorithm checks whether the distance between the bounding spheres is less than or equal to the sum of their radii. The generation of surface asperities is based on a multi-sphere approach. Here, defined surface asperities are created by placing small spherical particles onto the surface of a larger spherical particle, which are then bonded together. The contact force between neighboring particles is calculated based on their elemental spheres, using a sphere-to-sphere contact detection method (Wang et al. 2020). All parameters employed in the LIGGGHTS simulations are provided as supplementary information.

A stable time step is essential for integrating Newton's equations of motion. In this context, the Rayleigh time is used to estimate the necessary time step. The Rayleigh time represents the propagation of a wave that corresponds to the natural frequency of particles during an elastic collision (Norouzi et al. 2016). The time steps for the DEM were set to be no more than 10% of the Rayleigh time, ensuring the stability of the simulation (O'Sullivan et al. 2004).

The simulation setup for generating particle beds involves placing particles into a rectangular box, with periodic boundary conditions applied in the x- and y-directions to minimize wall effects. Particles that leave the simulation box on one side reenter the domain on the opposite side. Particles are introduced through an insertion face at the top of the simulation domain, while a fixed wall is implemented on the bottom (z-side) to facilitate the formation of a granular particle bed. Under gravity, particles settle in the negative z-direction. After all particles are settled, the particle bed is compressed with a stamp from the upper z-side. The compression continues until a set pressure is reached on the stamp. Preliminary simulations showed that after a pressure of 0.001 Pa, an increase in pressure does not yield any further compression. Thus, a maximum pressure of 0.1 Pa is set to guarantee maximal bed compression. The process of particle packing over time is shown in Fig. 1. Example simulation scripts for each particle type are provided in the supplementary information.

Three different particle types are utilized to investigate the effects of particle shape and surface asperities through simulation. These particles are prolate and oblate ellipsoids and spherical particles with defined surface asperities. An example particle of each type is shown in Fig. 2. The ellipsoids were generated using the superquadric library in LIGGGHTS. This approach simplifies the complex shapes of real non-spherical particles, enabling the investigation of particle shape effects based on defined convex geometries. Here, superquadrics provide a way to represent a complete boundary surface using a simple analytical equation (Williams et al. 1992). A three-dimensional superquadric particle can be described as follows:

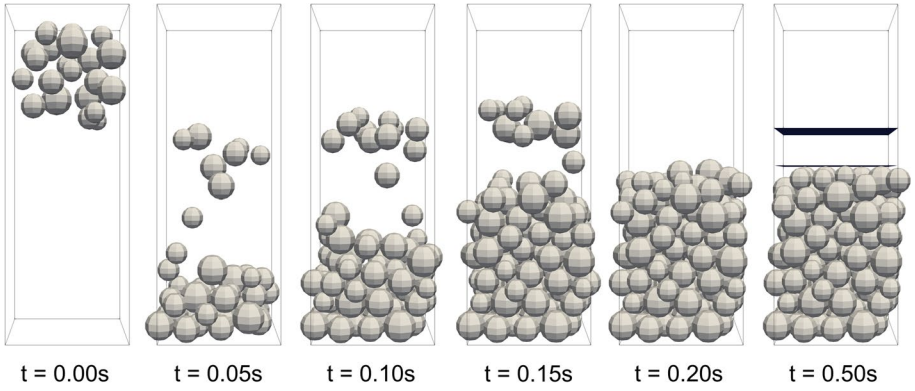

Fig. 1 Generation of a particle bed in LIGGGHTS. Particles are generated at height and settle under gravity. After the settling, the bed is compressed with a stamp

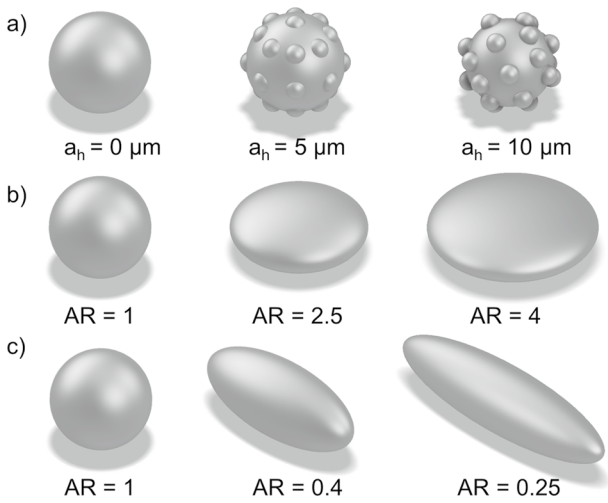

Fig. 2 Depiction of simulated non-spherical particle types: (a) rough spheroids with asperity heights between $a_h = 0 - 10\ \mu m$ (b), oblate ellipsoids with aspect ratios between $AR = 1 - 4$ (c), prolate ellipsoids with $AR = 0.25 - 1$

$$f(x,y,z) \equiv \left(\left| \frac{x}{a} \right|^{n_2} + \left| \frac{y}{b} \right|^{n_2} \right)^{n_1/n_2} + \left| \frac{z}{c} \right|^{n_1} - 1 = 0 \tag{6}$$

Here, x, y, and z represent the coordinates of points in the x-, y-, and z-directions. The parameters a, b, and c are the half-lengths of the superquadric particles, which control the stretching or compression of the particles along the main body axes in each spatial dimension. Ellipsoids with radii a, $b = a$, and c were generated at different aspect ratios (AR). The particle shape, which depends on the aspect ratio, is shown in Fig. 2. The aspect ratio is defined as the ratio of a to c, with $AR > 1$ resulting in oblate ellipsoids and $AR < 1$ resulting in prolate ellipsoids. When $AR = 1$, the radii are equal in all directions, resulting in a sphere.

The blockiness parameters n_1 and n_2 control the edge sharpness of a particle. As the blockiness increases, the particle shape becomes more convex. Theoretically, as the parameter tend to infinity, the particle shape approaches a perfect cuboid. Blockiness

parameters smaller than 2 would result in a concave shape, but such values are prohibited in the superquadric model in LIGGGHTS. For our simulation, we have chosen $n_1 = n_2 = 2$, resulting in an elliptical particle shape. The radii of the ellipsoids were calculated to result in a constant $x_v = 91.97\,\mu m$ at all AR. This volume equivalent particle diameter x_v corresponds to the value of a reference particle system shown in the supplementary information section.

Additionally, the behavior of the particle surface plays an important role for granular porous media. Particle roughness refers to irregularities or unevenness of a particle surface. The microscopic elevations on the surface are known as surface asperities, which influence properties such as friction, deformation, surface adhesion, and particle ploughing (Jiang et al. 2025). One parameter to describe the particle roughness dependent on surface asperities is the particle roughness ratio R_p (Jian-Chao et al. 2010; Ronoh et al. 2024; Zeng et al. 2025) which is defined as:

$$R_p = \frac{A_{\text{real}}}{A_{\text{smooth}}} = 1 + \frac{n\left(A_{\text{asp}} - A_{\text{base}}\right)}{A_{\text{smooth}}} \tag{7}$$

Here, A_{real} is the actual particle surface, A_{smooth} is the perfect smooth surface of a particle, A_{asp} is the surface of the asperity, A_{base} is the base area replaced on the smooth surface and n is the number of asperities. Individual microscopic surface asperities are generated as spherical segments on the particle surface, creating particle roughness. This approach simplifies the real surface irregularities on particles while enabling a detailed investigation of their influence. For spherical particles with defined surface asperities, which are also composed of spherical segments, a direct correlation can be established between the geometric parameters and the particle roughness ratio:

$$R_p = 1 + \frac{n\left(2r_a a_h - r_b^2\right)}{4r_p} \tag{8}$$

In this case, r_a is the radius of the asperity, a_h is the height of the surface asperity on the carrier particle, r_b is the radius of the base circle of the spherical segment forming the asperity, and r_p is the radius of the smooth carrier particle on which the asperities are generated. A surface roughness ratio $R_p > 1$ indicates an enlargement of the particle surface due to unevenness, while $R_p = 1$ represents a smooth particle surface.

Surface asperities were integrated by applying spots with a defined height on the particle surface using a multi-sphere model in LIGGGHTS. Small uniform spheres, so-called asperities, were distributed evenly on the surface of a core particle, see Fig. 2a. In this study, the number of asperities selected for analysis was fixed at 26, with each asperity having a diameter of 20 µm. The value of 26 was chosen to highlight the significant impact of surface asperities on porosity and permeability. The distribution of the asperities was determined using spherical coordinates, with the angles φ and θ set to 45°. This configuration, implemented via a MATLAB script ensured a constant number and distribution of the asperities.

Particles of different surface asperities were modeled by varying the amount the asperities protrude from the core particle. This parameter is called the asperity height. Particles with a_h values ranging from 0 to 100% of the asperity radius were simulated, corresponding to a_h values between 0 and 10 µm. The volume equivalent particle diameter was kept constant at all a_h values, with $x_v = 91.97\,\mu m$. This was accomplished by adjusting the core particle diameter while maintaining a constant asperity radius. The asperity height of

$a_h = 10\,\mu m$ results in $R_p = 1.34$, while $a_h = 0\,\mu m$ corresponds to $R_p = 1$, representing a completely smooth surface.

3.2 Analysis of Packing Homogeneity

In the process of extrapolating the simulation results to larger porous structures, the use of a homogeneous particle bed is essential. Inhomogeneities may arise due to variations in packing density. For the analysis of this condition, particle beds were divided into ten same sized segments. The porosity ε was then calculated for each segment. The packing density analysis was done for a bed of 1000 mono-sized spherical particles with $x_v = 91.97\,\mu m$. The porosity distribution across the bed height is shown in Fig. 3.

The granular porous structure shows a homogeneous packing density in the center of the bed with a significantly increased porosity in the lowest and highest segment. Excluding these values yields a porosity standard deviation of 2.0%. The changes in packing density at the top and bottom of the particle bed can be attributed to the wall effects. At the bottom segment, porosity increases by 16.8%. It can be observed in Fig. 3, that hollow spaces form between the particles and the bottom wall. The porosity is the highest in the top segment. It is increased by 26.5% compared to the average. Here, the stamp compressing the particle bed is stopped by the highest particles, leaving some empty spaces at the top. The deviations on both sides of the bed result from the geometry and are unavoidable, without

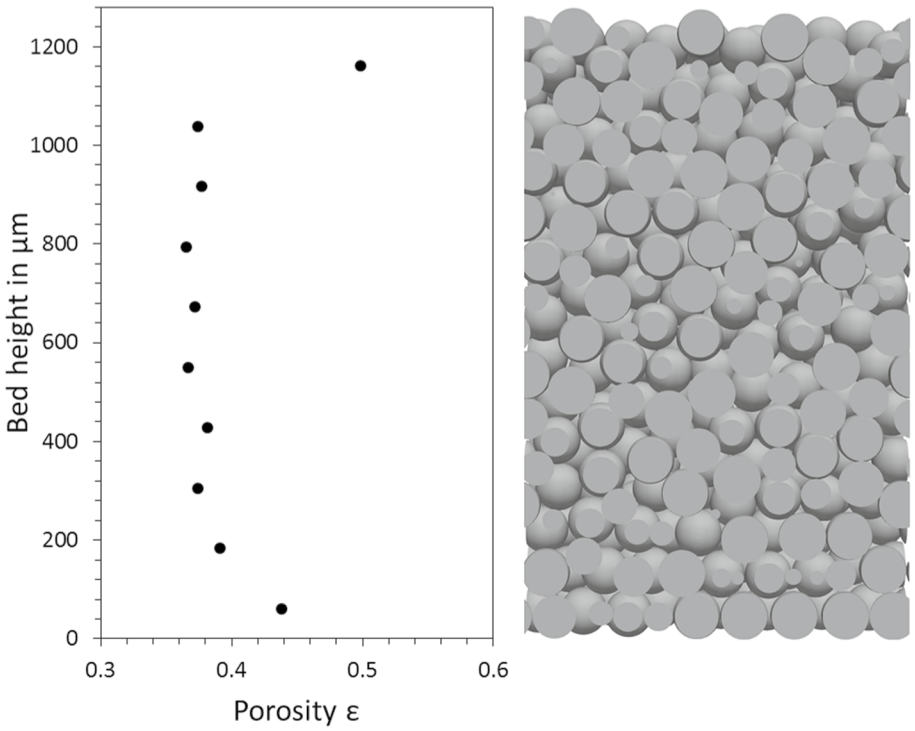

Fig. 3 Porosity over the bed height for a bed of monodisperse spherical particles along with an image of the analyzed bed

changing the properties of the particle bed. Areas of increased porosity could be reduced by cutting the geometry which would in turn also affect the simulation results. Cutting particle beds alters the shape and surface-to-volume diameter of the particles, which is why it is avoided in this work. The periodic boundary conditions applied to the sides of the computational domain during the DEM simulations eliminate wall effects in these regions, making variations in packing density along the sides of the particle bed unlikely. Therefore, it can be concluded that the height of the bed has a larger impact on the overall bed porosity than the side length. For the following simulations, the height to side length ratio of the particle beds is set to be larger than one, with the goal to reduce the effect of packing variability. The impact of the discussed inhomogeneities will decrease as bed size increases, since they occur only at the top and bottom layers. A sufficiently large particle number must be chosen to minimize the effect to an acceptable level.

3.2.1 Smallest Representative Particle Number Study

The goal of this work is to model the properties of real particle beds through simulation. A challenge arises from the fact that particle numbers in industrial processes are orders of magnitude higher than what can be simulated computationally. Therefore, a representative number of particles must be determined to allow for the extrapolation of results to much larger particle beds. In addition, the particle bed must be large enough to minimize the effect of the observed porosity changes at the top and bottom of the bed to an acceptable level. The impact of the number of simulated particles on the resulting bed properties is also investigated. For this purpose, beds of monodisperse spheres with $x_v = 91.97\ \mu m$ and particle numbers of 350, 1000, 1588, and 2032 were generated. The particle numbers were calculated relative to the simulation domain to maintain a consistent bed height-to-side length ratio across all simulations. This was achieved using the following equation:

$$N = N_0 \frac{d^3}{d_0^3} \tag{9}$$

Here, N_0 and d_0 are the particle number and side dimension of the smallest simulated particle bed volume. Additionally, d and N represent the corresponding values for the volume to be calculated. For each particle number, three particle beds were generated in LIGGGHTS. The resulting average porosity and standard deviation are presented in Fig. 4.

The porosity shows a decreasing trend with higher particle numbers. The highest average porosity $\varepsilon = 0.398$ is observed with the lowest particle number of 350, while the lowest value of ε was recorded at 2032 particles with 0.394. This is a slight decrease of 0.97%. Figure 3 shows that the porosity of the generated particle beds is increased at the top and bottom of each bed. The observed trend in porosity can be attributed to the diminishing influence of these areas in larger beds. To balance accuracy with computational cost, the particle number for the subsequent simulations with ellipsoid particles is set to 1000.

In LIGGGHTS, surface asperities are modeled using a multi-sphere approach, where each asperity is represented by a separate sphere. Consequently, the computational cost for simulating particles with asperities is 27 times higher than for spherical particles, given the same particle number. Surface asperities are smaller features on the particle surface. They require a finer mesh resolution, which in turn increases the computational effort for pore-scale simulations. Due to these constraints, a particle number of 350 was chosen for simulating granular porous media with asperity surfaces. The highest standard deviation relative to the average porosity occurs with 1588 particles, at 0.47%, while the average standard

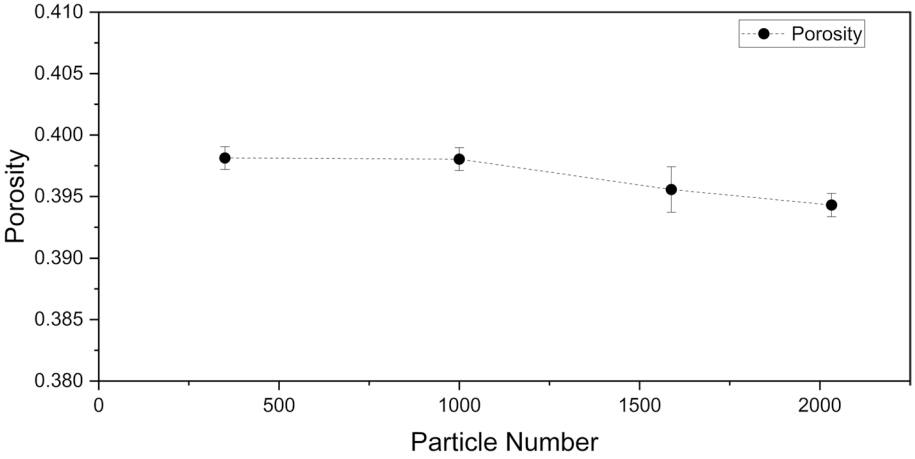

Fig. 4 Average porosity and standard deviation of beds with particles numbers between 350 and 2032

deviation is 0.29%. This demonstrates the high reproducibility of DEM simulations, indicating that generating multiple beds with the same properties is unlikely to significantly alter the simulation results. To minimize computational effort, all subsequent simulation experiments will be conducted only once.

Figure 5a illustrates the packing structure of the granular porous media as a function of aspect ratio for prolate and oblate particles. The ellipsoids align with their geometric characteristics within the bed, reflecting their shape and aspect ratio. This alignment not only affects porosity but also influences permeability, which is discussed in detail in Sect. 4.1. The impact of surface asperity on the packing structure is shown in Fig. 5b, with its effects on porosity and permeability further explored in Sect. 4.2.

3.3 Simulation Setup

3.3.1 CFD Simulation Setup in OpenFOAM

All pore-scale simulations were conducted using the open-source CFD software OpenFOAM. Here, the flow is simulated through the discrete solution of the Navier–Stokes equations based on the finite volume method (FVM) (Weller et al. 1998). The FVM divides the computational domain into a finite number of non-overlapping sub-volumes, referred to as cells. The Navier–Stokes equations are then reformulated into linear algebraic equations for each cell (Paschedag 2004).

The mesh generation for the pore-scale simulations was done with the pre-processing utility snappyHexMesh (SHM) in OpenFOAM. SHM enables the creation of 3D meshes from STL files. Mesh generation in SHM is carried out in 3 steps: (1) creation of a castellated mesh, (2) snapping of the cells to the geometry surface and (3) addition of surface layers. In the first step, the mesh adapts to the geometry by splitting cells and removing any cells outside the simulation domain. Refinement can be applied to selected geometry surfaces at this stage. The refinement is possible in multiple levels, whereas each level corresponds to a cell size reduction by a factor of eight. In the snapping stage, the vertex points of the jagged castellated mesh are moved to the surface geometry. The snapping process

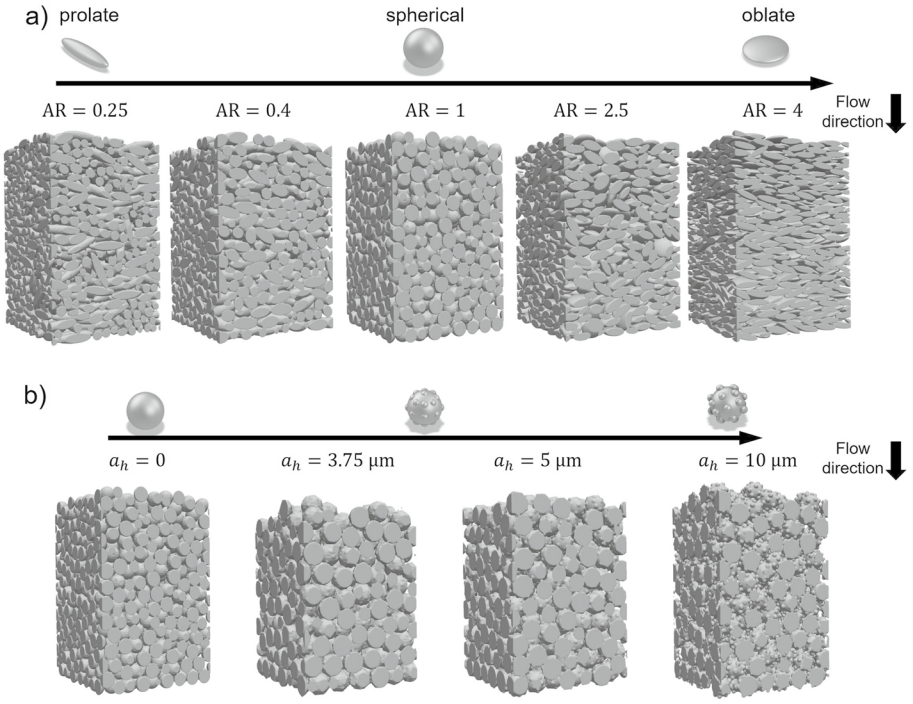

Fig. 5 Overview of the granular porous materials examined. (**a**) Influence of the aspect ratio on the structure of the aggregate. (**b**) Influence of the asperity height on the particle bed structure

takes place in several iterations with the aim of identifying displacements of the corner points that do not violate the parameters for mesh quality. In the last step, additional layers of hexahedral cells aligned to the boundary surface can be added (Weller et al. 1998). Because the snapping of the mesh to the complex particle bed geometries resulted in cell skewness above the warning threshold (>4) in the particle contact regions, both this step and the addition of surface layers were omitted in this work. For all pore-scale simulations, a castellated mesh with surface refinement around the particle surfaces was used. A castellated mesh consists of a structured grid of hexahedral cells.

For the pore-scale simulations, we use the pimpleFoam solver in OpenFOAM, which is a transient solver designed for simulating incompressible flows and Newtonian fluids (Moukalled et al. 2015). The fluid phase is an incompressible Newtonian fluid with a density ρ of 1000 $kg{\cdot}m^{-3}$ and a dynamic viscosity η of 10^{-6} $m^2{\cdot}s^{-1}$. The time step for each simulation is selected so that the maximum Courant number reached is less than one (Ferziger 2008). The simulations are run until a steady state is reached. No turbulence modeling is applied, as the flow through the porous particle bed is laminar. Additionally, gravity is set to -9.81 $m{\cdot}s^{-2}$ in the z-direction. The boundary conditions used for the simulation are reported in Table 2. To minimize the effect of the walls, the boundary condition cyclicAMI is implemented on the sides of the computational domain in the x- & y-directions. This condition allows the coupling of two patches that share the same outer bounds. Fluid that leaves the computational domain on one side reenters on the opposite side. The velocity at the inlet is set to a fixed value in the z-direction. On the outlet, the inletOutlet

Table 2 List of boundary conditions used in the CFD model in OpenFOAM

Parameter	Patch	Boundary Condition	value
Pressure in $m^2\ s^{-2}$	Inlet	zeroGradient	-
	Outlet	fixedValue	value uniform 0
	Walls	cyclicAMI	-
	Particles	fixedFluxPressure	-
Velocity in $m^1\ s^{-1}$	Inlet	fixedValue	Value uniform (0 0 u_z)
	Outlet	inletOutlet	inletValue uniform (0 0 0)
	Walls	CyclicAMI	-
	Particles	fixedValue	value uniform (0 0 0)

condition functions similarly to a zeroGradient condition, with the addition that it prohibits backwards flow through the patch back into the domain, which could lead to stability issues. At the particle surface, a no slip condition applies. The pressure at the inlet is set to zeroGradient, whereas the outlet has a set pressure of zero. On the particle surface, the fixedFluxPressure condition adjusts the pressure to the velocity for increased simulation stability. The initial values for both pressure and velocity were set to zero in all directions.

Embedding the particle structure within an isotropic porous zone minimizes the influence of inflow and outflow regions on the simulation results. The porous zone enhances numerical stability in the pore-scale simulations by homogenizing the flow velocity at the boundaries and reducing unphysical backflows. Implementing the porous media allows the inflow zone within the particle bed to be omitted, lowering computational cost. The embedding is achieved using the Darcy-Forchheimer model, which adds particle-free regions at the top and bottom of the bed. In OpenFOAM, a porous zone is defined by the Darcy coefficient (D) and the Forchheimer coefficient (F), both of which are calculated according to (10) and Eq. (11) to

$$D = 150\frac{(1-\varepsilon)^2}{\varepsilon^3}\frac{1}{x_{sv}^2} \tag{10}$$

$$F = 3.5\frac{1-\varepsilon}{\varepsilon^3}\frac{1}{x_{sv}} \tag{11}$$

The modified Kozeny coefficient of 150 in Eq. (10) is based on experimental investigations by Ergun et al. (1949), who found a lower value for real packings. For further details, see (Kramer et al. 2020). In addition, the cyclic connection of the geometric sides proved difficult for complex geometries. Embedding the particles in the same porous media on the sides allows the use of the cyclicAMI boundary condition. The size of the media was specified to be 30 µm on the sides, two times the 60 µm on top and 120 µm on the bottom. The added areas at top and bottom are not included in permeability calculations.

3.3.2 Mesh Independence Study

Discretization in CFD significantly influences the simulation results. To identify suitable meshing parameters, a mesh independence study was performed. For this purpose, a bed of 150 particles was used for each particle type. Specifically, ellipsoids with $AR = 4$ and

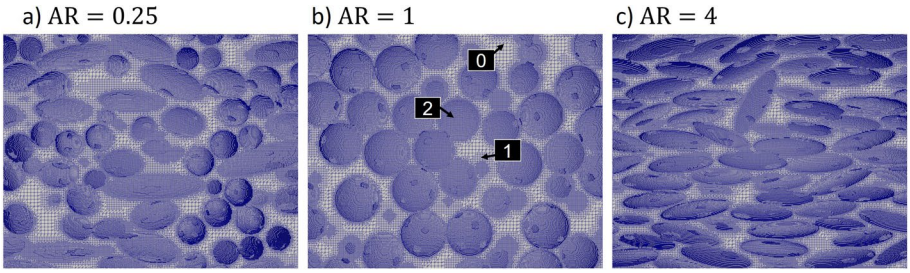

Fig. 6 Zoom on a sample mesh with two refinement levels. Cells of each refinement level and base cells (level 0) have been marked; (**a**) $AR = 0.25$; (**b**) $AR = 1$; (**c**) $AR = 4$

Table 3 Resulting error on permeability for different meshing strategies with ellipsoid and rough particles

No	Cells	Level	Error on K ($AR = 4$)	Error on K ($AR = 0.25$)	Error on K ($a_h = 10\,\mu m$)
A	16	1	0.59%	0.73%	−0.41%
B	20	1	−2.83%	−2.85%	3.09%
C	23	1	−3.07%	−1.84%	1.22%
D	26	1	−2.03%	−2.36%	1.42%
E	30	1	1.19%	0.56%	−1.05%
F	10	2	−0.81%	−1.37%	0.21%
G	13	2	−1.30%	−0.08%	−1.78%
H	16	2	1.51%	1.72%	1.12%
I	20	2	−1.73%	−1.65%	−2.63%
J	23	2	−0.23%	0.59%	−3.51%
K	26	2	0.39%	−0.26%	−0.13%
L	30	2	0.00%	0.00%	0.00%

$AR = 0.25$, as well as rough particles with $a_h = 10\ \mu m$, were selected. To capture the finest features of each particle type, which require the highest level of discretization, two mesh parameters were investigated for their effect on the simulated particle bed permeability. First, the number of base cells per volume-equivalent particle diameter was varied between 10 and 30. Additionally, mesh refinement levels (RL) between one and two were tested. A mesh with two refinement levels is shown in Fig. 6, with the cells of each RL labeled for clarity.

In total, 12 different meshing strategies (A-L) were examined. The parameters of the strategies are detailed in Table 3. The flow velocity for the simulations was calculated to result in a Reynolds number of one. After the simulations, the particle bed permeability K was calculated from the simulated pressure drop resulting from each meshing strategy. Table 3 reports the change of K in %. The simulated permeability with the different meshing strategies were compared to that of the one with the highest number of cells L of each particle type. Since this meshing strategy has the highest degree of discretization it has the most accurate results.

With one RL the error on K is higher and no convergence of the error can be observed. For the meshing strategies with 2 RL, the error hardly changes between the finest meshing strategies K & L. This indicates that an increase in cell count will not significantly impact

the simulation results. Therefore, two refinement levels were chosen for the simulations. A trade-off must be made between discretization accuracy and the total mesh size. Because SHM can only process a limited number of cells, the selected meshing strategy imposes an upper limit on the number of particles in the simulated beds. Therefore, it is essential to balance the discretization error with the error introduced by the bed size. For ellipsoids, all meshing strategies with two refinement levels (RL) result in deviations of no more than 1.72% from the finest meshes. For these particles, meshing strategy G was selected. This strategy demonstrated an error of − 1.3% for oblate ellipsoids and − 0.08% for prolate ellipsoids. For the rough particles, meshing strategy H was selected, resulting in an error of 1.12% compared to the finest mesh. The impact of discretization on the results is expected to be minimal for all particle types. It can be summarized that both the number of cells and the degree of refinement have an influence on the calculation time. As the number of cells and the degree of refinement increase, the volume elements in the grid become smaller and the simulation time increases.

4 Results and Discussion

4.1 Effect of Particle Shape on Filter Cake Properties

An important characteristic for the description of particles is the shape. Particles in industrial processes are seldom spherical (Müller 2021). Therefore, determining a relationship between particle shape parameters and bed properties is useful. In this chapter, the influence of the shape of ellipsoid particles on the porosity and flow permeability of the porous bed is investigated. Particle beds of ellipsoids with AR between 0.25 and 4 were generated as described in Sect. 3.1. Figure 7a presents the analysis of the pore-scale simulation

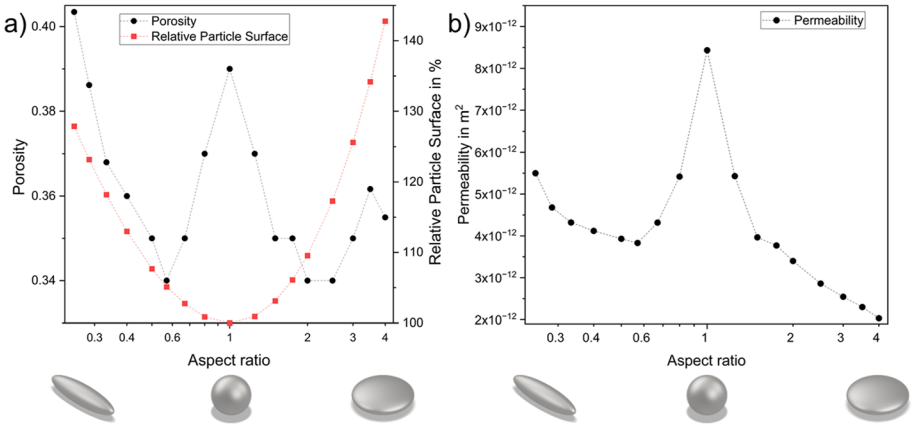

Fig. 7 **(a)** Comparison of the porosity ε and total particle surface area A_p. **(b)** particle bed permeability K for ellipsoids with $x_v = 91.97\ \mu m$ and $0.25 \leq AR \leq 4$

in relation to their porosity and total particle surface area A_p, for ellipsoid particles. As expected, the surface area of the spherical particles is the smallest.

The total particle surface area increases exponentially with morphological change for both prolate and oblate ellipsoids. The increase in surface area is less rapid in the prolate particles. Here, A_p is increased by 27.9% at an $AR = 0.25$ compared to spherical particles. At the corresponding $AR = 4$ of the oblate ellipsoids, this increase amounts to 42.8%.

The porosity ε has a maximum for the spherical particles at an $AR = 1$. The trend of ε follows a parabolic shape for both prolate and oblate ellipsoids. The observed minima of the porosity are at an $AR = 1/1.75$ for the prolate ellipsoids and $AR = 2$ for the oblate ellipsoids. The qualitative trend of the porosity observed here is consistent with the findings of Zhou et al. (2011). In their study, Zhou et al. (2011) identified porosity minima at AR = 1/1.67 and AR = 1.8 using DEM, which aligns with the data presented here. Therefore, it can be concluded that the simulation setup provides valid results. At least two opposing factors seem to influence the porosity in relation to the aspect ratio. Close to $AR = 1$, the change in shape allows for a denser packing. The analysis of ordered particle configurations shows that ellipsoids can be packed to higher solids volume fractions than spheres (Donev et al. 2004). The observed increase in ε for $AR < 1/1.75$ and $AR > 2$ could be explained with a higher bulkiness of the particles The prolate and oblate ellipsoids have a higher extent, which could cause a less dense packing.

CFD simulations were carried out through each ellipsoid geometry at $Re = 1$. The determined pressure drop through the geometry was used to calculate the bed permeability K in relation to the aspect ratio of the ellipsoids. The results are displayed in Fig. 7b. The maximum permeability was observed for spherical particles with an $AR = 1$. For the prolate ellipsoids, a parabolic trend of K can be observed. The permeability decreases with a decreasing sphericity until K reaches a minimum at $AR = 1/1.75$. For $AR < 1/1.75$ the permeability increases again. The observed trend in porosity for prolate particles, which reaches a minimum at an aspect ratio of 1/1.75, suggests that a lower porosity corresponds to an increase in pressure loss through the particle bed (Sorrentino 2002). This trend can be attributed to an increase in capillary pressure within the particulate structure, resulting from smaller pore volumes. Another key factor influencing the permeability trend is the specific surface area of the particles. A higher particle surface area decreases permeability. This explains the slower increase of K for $AR < 1/1.75$ compared to the increase in porosity. The trend for the oblate ellipsoids shows a slowing exponential decline with an increasing AR. In contrast to the prolate ellipsoids, the permeability further decreases after the minima of ε is passed. The reason for this is most likely the lower porosity and higher surface area compared to the prolate ellipsoids. At an A $R = 1.25$ and $AR = 1/1.25$ the permeability of the prolate and oblate ellipsoids is similar, with a 0.25% higher value of K for the oblate particles. For all other corresponding aspect ratios, the oblate particles have a lower permeability. The reasons for this are most likely the presented differences in A_p and ε.

4.2 Effect of Asperity Height on Filter Cake Properties

The second particle characteristic under investigation is the surface asperity. The previously simulated particles were assumed to be perfectly smooth. In contrast, rough particles with surface asperities ranging from 0 to 10 µm were generated, based on the asperity model outlined in Sect. 3.1. After conducting DEM simulations, the effect of asperity height on the properties of the particle bed was analyzed. The porosity and total surface area of the resulting beds were evaluated as a function of a_h.

It is noteworthy that the investigation of surface asperities through the integration of smaller spherical segments onto the surface of larger spherical particles is a simplification of actual particle surface properties. The incorporation of real surface properties could be achieved using imaging techniques such as micro-computed tomography. However, this approach lies outside the scope of the present investigation. Nonetheless, the integration of defined surface asperities enables the investigation of the impact of asperity height on specific surface area, particle bed porosity, and permeability.

The simulation results are depicted in Fig. 8a. As expected, an increase in asperity height leads to a higher particle surface area, as a larger proportion of the total particle volume is occupied by the surface asperities. It is evident that these smaller spheres possess a higher surface-to-volume ratio, which consequently results in an increase in the overall surface area of the particle. A_p shows an exponential growth in relation to a_h. Compared to the surface of smooth spheres, the total surface area is 27.85% higher when the maximum asperity height reaches 10.0 µm.

The porosity also exhibits an increasing trend with higher asperity heights. For perfectly smooth spheres ($a_h = 0\,\mu m$), the porosity is $\varepsilon = 0.40$. With the maximum asperity height of $a_h = 10.0\,\mu m$, the porosity increases to 0.49, representing a 23.14% rise compared to the smooth spheres. This increase in porosity can be attributed to several factors. First, the voids created by the surface irregularities are unlikely to be fully occupied by adjacent particles, resulting in an increase in the total void volume. Second, the roughness of the particles may influence the packing process. The asperities could cause the particles to interlock, reducing their mobility. As a result, particles would be less able to fill the empty spaces in the bed during packing. Additionally, the rearrangement of particles during bed compression could be hindered.

Pore-scale simulations were carried out using the generated particle beds to analyze the effect of changes in a_h on the bed permeability K. The pressure drop across the particle beds at $Re = 1$ was simulated, and the corresponding values for the bed permeability were calculated. Figure 8b shows the permeability as a function of asperity height. No clear trend in the permeability is observed between smooth spheres ($a_h = 0\,\mu m$) and rough

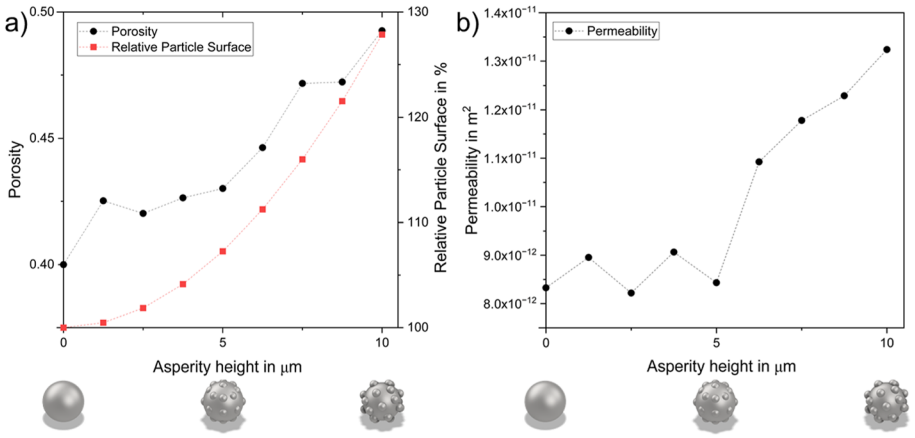

Fig. 8 Comparison of porosity ε and total particle surface area A_p (**a**) and permeability K (**b**) of particle beds with $x_v = 91.97\,\mu m$ in relation to the asperity height of the particles between 0 µm and 10 µm

particles with $a_h = 5\,\mu m$. The increase in porosity appears to be offset by the rise in particle surface area. However, as a_h increases further, permeability increases sharply, reaching a maximum at $a_h = 10\,\mu m$. At this point, permeability is 59% higher compared to smooth spheres. For these particles, the influence of increased porosity seems to outweigh the additional drag resulting from the larger surface area.

4.3 Comparison of Simulation Results with Empirical Equations

Empirical equations for the prediction of fluid behavior in porous particle beds contain significant uncertainties and can lead to considerable mistakes, if used in areas that are not directly proven by experiments (Rumpf et al. 1971). The permeability predictions of the widely used Carman-Kozeny and Ergun equations were compared to the generated simulation results to investigate the applicability of these equations for different particle types. The simulated permeabilities of the ellipsoid particle beds and the corresponding empirical predictions of the Ergun and Carman-Kozeny equations are shown in Fig. 9 over the aspect ratio.

The Carman-Kozeny equation shows high alignment with the simulated data with an average absolute deviation of 8.7%. For perfect spheres, Carman-Kozeny predicts a 10.0% lower K than the simulations. With all tested prolate ellipsoids, this difference is lower than 11%, indicating the validity of the equation for this particle type up to a low sphericity. Comparing the oblate ellipsoids, a high alignment can be observed up to an $AR = 2$, with all differences being smaller than 8.5%. The greatest observed deviations of the Carman-Kozeny equation to the simulations are seen at the highest aspect ratios, with 22.23% at $AR = 3.5$ and 18.0% at $AR = 4.0$. This could suggest that Carman-Kozeny produces slightly less accurate results for oblate particles with lower sphericities. More data is needed to test the limits of the equation. Overall, these results demonstrate the validity of Carman-Kozeny for non-spherical particles in the investigated area.

The Ergun equation deviates upwards from the simulation results for all values. The average deviation amounts to 36.7%. For perfect spheres, the Ergun equation shows a

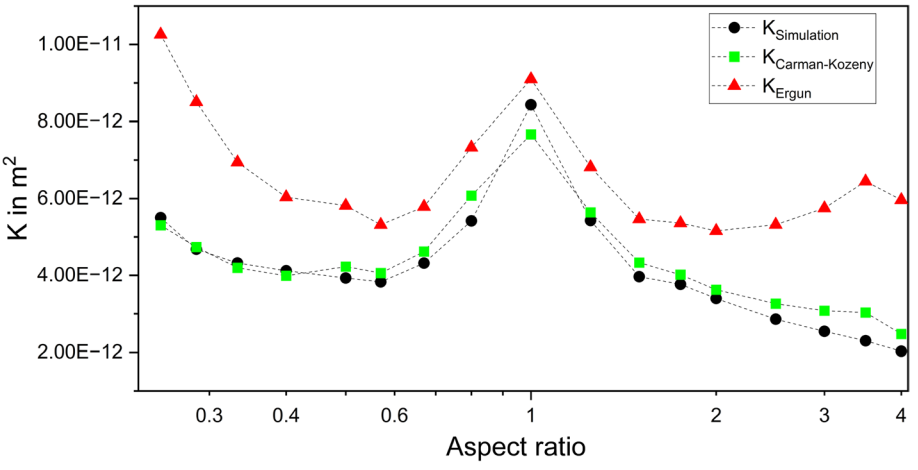

Fig. 9 Comparison of the simulated permeability with the empirical Carman-Kozeny and Ergun equations for ellipsoid particle beds with aspect ratios between 1/4 and 4

higher alignment than Carman-Kozeny with a deviation of 7.3%. Looking at the tested ellipsoids with the highest sphericities $\psi > 0.99$ at $AR = 1.25$ and $AR = 1/1.25$, the deviation increases to 20.36% and 26.1% respectively. It can be observed that the deviation of the Ergun equation increases with decreasing particle sphericity. For prolate ellipsoids, the deviation reaches its maximum at $AR = 1/4$ with 46.4%. With the oblate ellipsoids, the highest deviation of 65.9% can be observed at the highest $AR = 4$. These results suggest that while the Ergun equation is useful for describing spheres, even small deviations in shape can lead to an overestimation of permeabilities. It is important to note that the Ergun equation is applicable to steady, incompressible flow through homogeneous, isotropic particle beds composed of spherical particles. Therefore, the Ergun equation provides good agreement at an aspect ratio of $AR = 1$, corresponding to spherical particles. However, to accurately model non-spherical particles, the coefficients of the Ergun equation must be adjusted. This extension is beyond the scope of the present study. Therefore, the Ergun model should be used with caution when dealing with non-spherical particles. This limitation is likely due to the use of the volume-equivalent diameter in the Ergun equation, in contrast to the Sauter diameter employed in the Carman-Kozeny equation. As a result, the increased friction associated with the larger surface area of non-spherical particles is not accounted for in the Ergun model.

To examine the correlation between the simulation results and the empirical equations, the simulated permeability values were compared to the predictions from the empirical models (see Fig. 10). A function through the origin with a slope of one, which indicates a perfect correlation between simulation and equation, was added to the graphs. The Root Mean Square Error of the data points normalized by the average porosity (NRMSD) to this function was calculated. Additionally, the variance of the data points was marked with two linear functions through the origin that encapsulate all data points.

The Carman-Kozeny equation shows a high correlation to the simulation results with a NRSMD of 0.097. The variance of the data points is smaller here, with a ratio of 1.4 of the slopes of the functions that encapsulate the data points. The Ergun equation shows 6.5 times higher NRSMD = 0.634. Since the equation predicts a higher permeability than the simulations, all data points lay below the ideal function. Additionally, a higher variance can be observed with a ratio of 2.6 of the function slopes that encapsulate the data set. This underscores the applicability of the Carman-Kozeny equation for non-spherical particles,

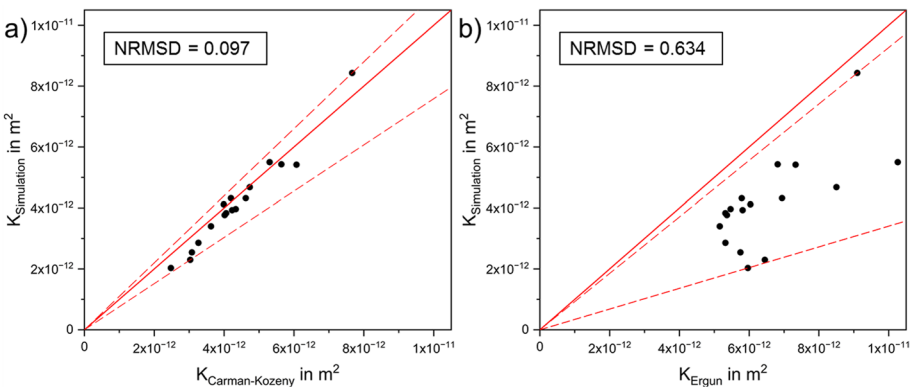

Fig. 10 Simulated permeability over Ergun prediction (**a**) and over Carman-Kozeny Equation (**b**) of ellipsoid particles beds with aspect ratios between 1/4 and 4

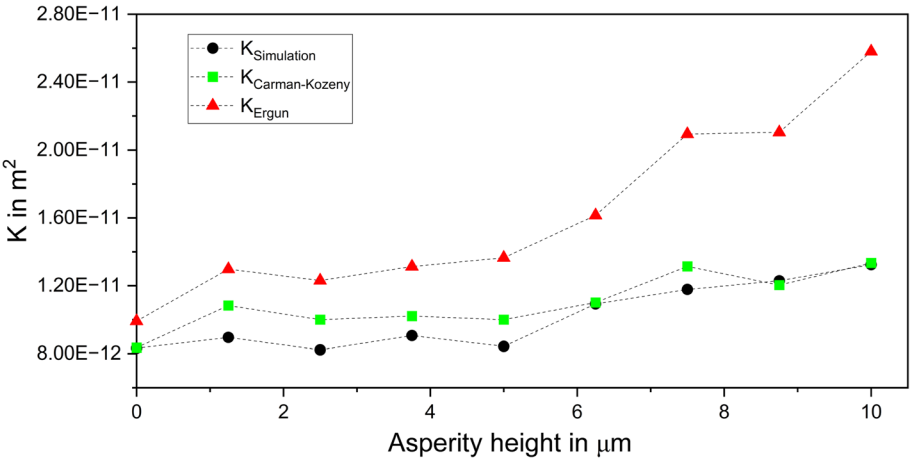

Fig. 11 Comparison of the simulated permeability with the empirical Carman-Kozeny and Ergun equations for rough particle beds with asperity heights between 0 and 10 µm

while the Ergun equation is not best suited for this area. The results of the simulations with rough particles were compared to the permeability predictions of the selected equations in Fig. 11.

The Carman-Kozeny equation presents a good alignment to the simulation results with an average absolute deviation of 8.5%. For smooth spheres the equation deviates by 0.3%. The difference of this value compared to the perfect spheres in the ellipsoid data set can be explained with the different bed sizes. While the differences between the datasets should be considered, they are expected to be sufficiently small to permit a valid evaluation of the empirical equations. For the highest asperity height, the deviation of the equation from the simulation results is only 0.8%. Additionally, all differences are observed to be below 18%. This demonstrates that the Carman-Kozeny equation is applicable to particles with a high degree of roughness. The Ergun equation demonstrates a tendency to overpredict permeability for all data points. The average deviation lays at 35.1%. The differences increase with increasing particle roughness, reaching the maximum at $a_h = 10\mu m$ with 48.7%. The reason for this is likely the neglected increase in particle surface as explained above. This shows that the Ergun equation should not be used when dealing with particles that have a high degree of roughness.

The simulated permeability of the rough particles was graphed over the predictions of the Carman-Kozeny and Ergun equations respectively in Fig. 12, as explained above. Carman-Kozeny shows a high correlation to the simulations with a NRMSD = 0.116. The variance of the results is low with a ratio of 1.2 of the functions slopes that encapsulate the data set. The error of the Ergun equation is 5.8 times higher with a NRMSD = 0.678. Additionally, the variance is higher here with a ratio of 1.6 of the function slopes. This confirms the applicability of the Carman-Kozeny equation for rough particles. The Ergun equation has only limited validity for this particle type.

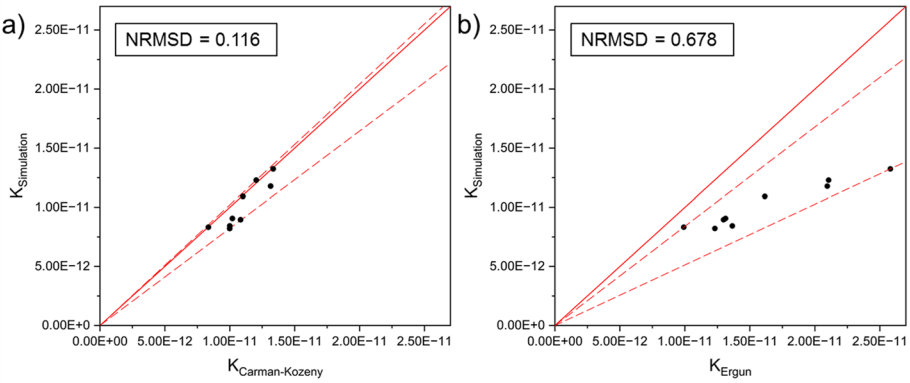

Fig. 12 Simulated permeability over Ergun prediction (**a**) and over Carman-Kozeny Equation (**b**) of ellipsoid particles beds with aspect ratios between 1/4 and 4

5 Conclusions

This article presents pore-scale simulations to describe flow through granular porous media. An investigation was carried out to examine the effect of particle shape and surface asperities on the resulting particle bed properties, including porosity, total surface area, and permeability. A DEM simulation setup for generating particle beds in LIGGGHTS was presented. The particles are arranged in a rectangular box with periodic boundary conditions on the sides. Following the settling of the particles, the bed is compacted using a stamp to enhance packing homogeneity. The model was modified to simulate different types of particles. Ellipsoids with varying aspect ratios can be simulated through the superquadric modeling of the particles. Rough particles with constant asperity distributions and varied asperity heights were modelled with by applying a multi-sphere approach. Sufficient particle bed sizes were found through a representative elementary volume study. To perform pore-scale simulations on the generated particle beds, an OpenFOAM model was utilized. Both DEM and CFD analyzes were conducted to evaluate the particle bed porosity and permeability, incorporating the effects of particle shape and surface asperity. The results aligned with physical expectations and were consistent with prior research. To assess the applicability of the empirical equations to the tested particle shape characteristics, the commonly used Carman-Kozeny and Ergun equations were compared to the simulation results. The findings revealed that the Carman-Kozeny equation provides accurate predictions for non-spherical particles.

For ellipsoid particles with aspect ratios between 0.25 and 4, as well as for rough particles up to the highest tested roughness the equation never deviated more than 23% from the simulation results and showed average deviations smaller than 9%. This indicates that the Carman-Kozeny equation is valid over a wide range of particle shapes. While the Ergun equation could show satisfactory accuracy for spherical particles, the deviations significantly increased with decreasing sphericity. For both rough and ellipsoid particles, the equation showed an average error of over 35% and individual deviations of up to 66% for the tested particles with the lowest sphericity. This demonstrates that the Ergun equation in this shape should only be employed if spherical particles are known to be present. Future studies could investigate more particle shapes like cylindrical or cuboid particles. Of interest is, if the surface-volume diameter is sufficient to describe the particle shape or if more

parameters need to be considered. Additionally, more empirical equations could be tested over a wider range of Reynolds numbers.

In conclusion, pore-scale simulations prove to be a valuable tool for studying flow through porous media. The results generated from the simulations are promising, and the approach developed in this work provides a deeper understanding of how particle properties influence flow behavior in porous media. Further work should focus on validating the simulation results and incorporating real surface roughness to gain a deeper understanding of how real surface irregularities affect the packing structure and permeability of granular porous media.

Supplementary Information The online version contains supplementary material available at https://doi.org/10.1007/s11242-025-02267-0.

Acknowledgements We acknowledge the support by the state of Baden-Wuerttemberg through bwHPC and by the KIT-Publication Fund of the Karlsruhe Institute of Technology.

Author contributions Conceptualization: P.W., M.G., Methodology: P.W.; Formal analysis and investigation: P.W.; Writing—original draft preparation: P.W., M.G.; Writing—review and editing: P.W., M.G.; Funding acquisition: H.N.; Resources: H.N., J.C.; supervision: J.C., M.G.

Funding Open Access funding enabled and organized by Projekt DEAL. The authors would like to thank the Deutsche Forschungsgemeinschaft DFG (German Research Foundation)—Project number: 504852622 for the financial support funding the project in the priority program PP2364 autonomous processes in particle technology.

Data availability The datasets generated during and analyzed during the current study are available from the corresponding author on reasonable request.

Declarations

Competing interest The authors declare that they have no known competing financial interests or personal relationships that could have appeared to influence the work reported in this paper.

References

Anlauf, H., Sorrentino, J.A.: The influence of particle collective characteristics on cake filtration results. Chem. Eng. Technol.: Indus. Chem.-Plant Equip.-Process Eng.-Biotechnol. **27**, 1080–1084 (2004)

Bai, H., Theuerkauf, J., Gillis, P.A., Witt, P.M.: A coupled DEM and CFD simulation of flow field and pressure drop in fixed bed reactor with randomly packed catalyst particles. Ind. Eng. Chem. Res. **48**, 4060–4074 (2009)

Carman, P.C.: Fluid flow through granular beds. Trans. Inst. Chem. Eng. Lond. **15**, 150–156 (1937)

Donev, A., Stillinger, F.H., Chaikin, P.M., Torquato, S.: Unusually dense crystal packings of ellipsoids. Phys. Rev. Lett. **92**, 255506 (2004)
Dong, K.J., Zou, R.P., Yang, R.Y., Yu, A.B., Roach, G.: DEM simulation of cake formation in sedimentation and filtration. Miner. Eng. **22**, 921–930 (2009)
Ergun, S., Orning, A.A.: Fluid flow through randomly packed columns and fluidized beds. Ind. Eng. Chem. **41**, 1179–1184 (1949)
Ferziger, J.H., Perić, M.: Numerische Strömungsmechanik. Springer, Berlin (2008)
Hommel, J., Coltman, E., Class, H.: Porosity–permeability relations for evolving pore space: a review with a focus on (bio-) geochemically altered porous media. Transp. Porous Media **124**, 589–629 (2018)
Jian-Chao, C., Bo-Ming, Y., Ming-Qing, Z., Mao-Fei, M.: Fractal analysis of surface roughness of particles in porous media. Chin. Phys. Lett. **27**, 24705 (2010)
Jiang, H., Nie, J., Debanath, O.C., Li, Y.: Dynamic column collapse of dry granular materials with multi-scale shape characteristics. Comput. Geotech. **177**, 106873 (2025)
Kerimov, A., Mavko, G., Mukerji, T., Dvorkin, J., Al Ibrahim, M.A.: The influence of convex particles' irregular shape and varying size on porosity, permeability, and elastic bulk modulus of granular porous media: insights from numerical simulations. J. Geophys. Res. Solid Earth **123**, 10–563 (2018)
Kramer, O.J.I., Padding, J.T., van Vugt, W.H., de Moel, P.J., Baars, E.T., Boek, E.S., van der Hoek, J.P.: Improvement of voidage prediction in liquid-solid fluidized beds by inclusion of the Froude number in effective drag relations. Int. J. Multiphase Flow **127**, 103261 (2020)
Kumar, P., Saha, S.K., Sharma, A.: Experimental and CFD-DEM study on local packing distribution and thermofluidic analysis of binary packed bed. Chem. Eng. Sci. **282**, 119372 (2023)
Li, D., Chen, J.: Mechanics of oil and gas flow in porous media. Springer, Berlin (2021)
Li, Y., He, G., Yu, B., Yan, S., Xie, L.: Dem-cfd modeling and simulations of hydrodynamic characteristics and flow resistance coefficient in fixed-bed reactors. Chem. Eng. J. Adv. **8**, 100167 (2021)
Lu, G., Third, J.R., Müller, C.R.: Discrete element models for non-spherical particle systems: from theoretical developments to applications. Chem. Eng. Sci. **127**, 425–465 (2015)
Mahdi, F.M., Hunter, T.N., Holdich, R.G.: A study of cake filtration parameters using the constant rate process. Processes **7**, 746 (2019)
Marcato, A., Boccardo, G., Marchisio, D.: From computational fluid dynamics to structure interpretation via neural networks: an application to flow and transport in porous media. Ind. Eng. Chem. Res. **61**, 8530–8541 (2022)
Molerus, O., Pahl, M.H., Rumpf, H.C.H.: Die Porositätsfunktion in empirischen Gleichungen für den Durchströmungswiderstand im Bereich Re⩽ 1. Chem. Ing. Tech. **43**, 376–378 (1971)
Moukalled, F., Mangani, L., Darwish, M.: The finite volume method. In: The finite volume method in computational fluid dynamics: An advanced introduction with OpenFOAM® and Matlab, pp. 103–135. Springer International Publishing, Cham (2015)
Müller W., Mechanische Verfahrenstechnik Und Ihre Gesetzmäßigkeiten, Walter de Gruyter GmbH \& Co KG, 2021.
Nield, D.A., Bejan, A.: Convection in porous media. Springer, New York (2006)
Norouzi, H.R., Zarghami, R., Sotudeh-Gharebagh, R., Mostoufi, N.: Coupled CFD-DEM modeling: Formulation, Implementation and application to multiphase flows. John Wiley & Sons, Hoboken (2016)
O'Sullivan, C., Bray, J.D.: Selecting a suitable time step for discrete element simulations that use the central difference time integration scheme. Eng. Comput. **21**, 278–303 (2004)
Paschedag A.R., CFD in Der Verfahrenstechnik: Allgemeine Grundlagen Und Mehrphasige Anwendungen, Wiley-VCH, 2004.
Podlozhnyuk, A., Pirker, S., Kloss, C.: Efficient implementation of superquadric particles in discrete element method within an open-source framework. Comput. Part. Mech. **4**, 101–118 (2017)
Qiu, J., Khalloufi, S., Martynenko, A., Van Dalen, G., Schutyser, M., Almeida-Rivera, C.: Porosity, bulk density, and volume reduction during drying: review of measurement methods and coefficient determinations. Drying Technol. **33**, 1681–1699 (2015)
Rhodes, M.J. (ed.): Introduction to particle technology. John Wiley & Sons, Hoboken (2008)
Richardson, J.F., Zaki, W.N.: The sedimentation of a suspension of uniform spheres under conditions of viscous flow. Chem. Eng. Sci. **3**, 65–73 (1954)
Rong, L.W., Dong, K.J., Yu, A.B.: Lattice-Boltzmann simulation of fluid flow through packed beds of uniform spheres: effect of porosity. Chem. Eng. Sci. **99**, 44–58 (2013)
Ronoh, K., Novotn\`y, J., Mr\vna, L., Knápek, A., Sobola, D.: Effects of laser and scanning parameters on surface modification of MONEL®alloy 400 by picosecond laser. Opt. Laser Technol. **172**, 110514 (2024)
Rumpf, H.C.H., Gupte, A.R.: Einflüsse der Porosität und Korngrößenverteilung im Widerstandsgesetz der Porenströmung. Chem. Ing. Tech. **43**, 367–375 (1971). https://doi.org/10.1002/cite.330430610

Schulz, R., Ray, N., Zech, S., Rupp, A., Knabner, P.: Beyond Kozeny–Carman: predicting the permeability in porous media. Transp. Porous Media **130**, 487–512 (2019)
Sorrentino, J.A.: From particle collective characteristics to cake permeability: the use of the pore-particle shape factor. Part. Part. Syst. Charact. **24**, 97–100 (2007). https://doi.org/10.1002/ppsc.200601047
Sorrentino J.A., Advances in Correlating Filter Cake Properties with Particle Collective Characteristics, Shaker Verlag, 2002.
Steenweg, C., Habicht, J., Wohlgemuth, K.: Continuous isolation of particles with varying aspect ratios up to thin needles achieving free-flowing products. Crystals **12**, 137 (2022)
Wang, X., Li, B., Xia, R., Ma, H.: Engineering applications of discrete element method. Springer, Singapore (2020)
Weller, H.G., Tabor, G., Jasak, H., Fureby, C.: A tensorial approach to computational continuum mechanics using object-oriented techniques. Comput. Phys. **12**, 620–631 (1998)
Whitaker, S.: Flow in porous media I: a theoretical derivation of Darcy's law. Transp. Porous Media **1**, 3–25 (1986)
Williams, J.R., Pentland, A.P.: Superquadrics and modal dynamics for discrete elements in interactive design. Eng. Comput. **9**, 115–127 (1992)
Xu, W., Zhang, K., Zhang, Y., Jiang, J.: Packing fraction, tortuosity, and permeability of granular-porous media with densely packed spheroidal particles: monodisperse and polydisperse systems. Water Resour. Res. **58**, e2021WR031433 (2022)
Zeng, H., Sun, W., Tang, H., Jiang, F., Wang, L.: Surface roughness and its role in flotation behavior, wettability, and bubble-particle interactions: a systematic review. Appl. Sci. **15**, 4557 (2025)
Zhang, Z., Yin, T., Huang, X., Dias, D.: Slurry filtration process and filter cake formation during shield tunnelling: insight from coupled CFD-DEM simulations of slurry filtration column test. Tunn. Undergr. Space Technol. **87**, 64–77 (2019)
Zhao, Y., Jiang, M., Liu, Y., Zheng, J.: Particle-scale simulation of the flow and heat transfer behaviors in fluidized bed with immersed tube. AIChE J. **55**, 3109–3124 (2009)
Zhou, Z.-Y., Zou, R.-P., Pinson, D., Yu, A.-B.: Dynamic simulation of the packing of ellipsoidal particles. Ind. Eng. Chem. Res. **50**, 9787–9798 (2011)